Towards Accurate Amplitudes for One-way Wavefield Extrapolation of 3-D Common Shot Records

Yu Zhang, James Sun, Samuel H. Gray, Carl Notfors, Veritas DGC Inc., and Norman Bleistein, Colorado School of Mines

Summary

We analyze the amplitudes produced by shot-record migration by one-way wavefield extrapolation. By comparing these amplitudes with those produced by true-amplitude Kirchhoff migration, we show the amplitude and phase errors that come from a standard implementation of migration by one-way wavefield extrapolation. Next, we present a new formulaton of shot-record migration that maintains its high fidelity in imaging complex structures, has correct dynamic behavior at least for constant velocity, and can be easily extended to $v(z)$. This formulation requires that we modify, in a straightforward way, the wavefield that is being downward continued. Our analysis applies equally to all migration methods based on one-way wavefield extrapolators.

Introduction

Until recently, Kirchhoff migration has been used for most 3-D prestack migrations, primarily because of its versatility and efficiency. The demands of imaging increasingly complex geological structures, however, have spurred a demand for increased imaging fidelity. This has led to the growing popularity of imaging methods that handle more than the single arrival (e.g., maximum-energy) that Kirchhoff migration is capable of handling conveniently. Such methods include multi-arrival Kirchhoff migration, which allows for several arrivals at each image location, and finite-difference migration, which allows for an unlimited number of arrivals at each image location. In this paper, we concentrate on one-way wavefield extrapolation, paying particular attention to its amplitude and phase behavior.

The standard formulation of finite-difference migration (Claerbout, 1985) consists of two parts. The first part is the downward continuation of the wavefields from the source and receiver locations using a "wave equation" that splits the wavefields into downgoing and upgoing parts. The second part is the application of an imaging condition, namely the division of the downward continued receiver wavefield by the downward continued source wavefield at each image point. Unfortunately, the one-way "wave equations" used in the downward continuation are not equivalent to the acoustic wave equation whose behavior they are designed to mimic. This lack of equivalence leads to a migrated wavefield that lacks correct amplitude and phase behavior, even though it is kinematically correct. By expressing the downward continued wavefields asymptotically, we are able to compare the imaged wavefield with the reflection coefficient of true amplitude Kirchhoff migration. The latter is our benchmark for amplitude and phase. The former is the downward continued receiver wavefield divided by the downward continued source wavefield. This comparison leads to a corrected equation for the upgoing and downgoing wavefields which, in turn, leads to a corrected expression for the wavefields being downward continued. When these corrections are applied, the migration produces images whose amplitudes and phases agree with true-amplitude Kirchhoff migration. These corrections are essentially without cost, and they do not compromise the migration's structural imaging fidelity, such as finite-difference migration.

Theory

We begin with a layered velocity ($v(z)$) earth and 3D common-shot migration. Given an acoustic wave-field p with source excitation at $\vec{x_s} = (x_s, y_s, 0)$ and $t = 0$,

$$\left(\frac{1}{v^2}\frac{\partial^2}{\partial t^2} - \frac{\partial^2}{\partial z^2} - \triangle\right) p(x, y, z; t) = \delta(\vec{x} - \vec{x_s})\delta(t), \quad (1)$$

(where $\triangle = \frac{\partial^2}{\partial x^2} + \frac{\partial^2}{\partial y^2}$), we record the surface data Q:

$$p(x_r, y_r, z = 0; t) = Q(x_r, y_r; t). \quad (2)$$

According to Bleistein et al.'s (2001) work on inversion, the true-amplitude common shot Kirchhoff inversion formula is (Zhang et al., 2000)

$$R(x, y, z) \sim \iiint i\omega \frac{\sqrt{\cos\alpha_{s0}\cos\alpha_{r0}}}{v_0}\sqrt{\frac{\psi_s\sigma_s}{\psi_r\sigma_r}} \; e^{i\omega(\tau_s+\tau_r)}\hat{Q}(x_r, y_r; \omega)dx_r dy_r d\omega, \quad (3)$$

where ψ and σ are in-plane and out-of-plane geometrical spreading terms and α_{s0} and α_{r0} are surface angles at

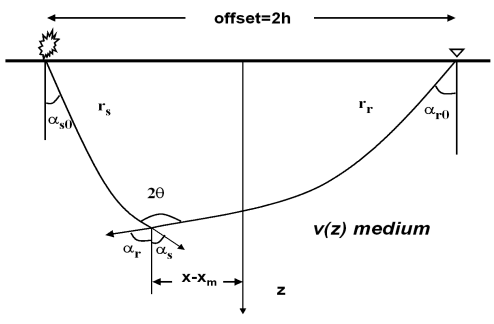

Fig. 1: Ray paths in a $v(z)$ medium.

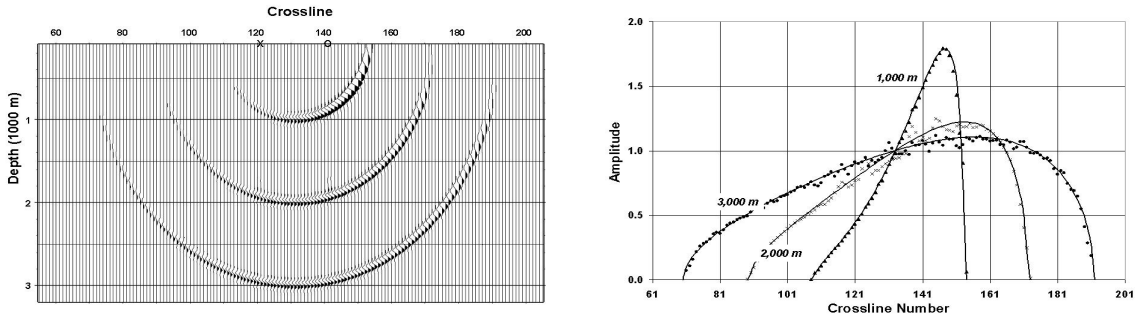

Fig. 2: Left: 3-D phase-shift migrated impulse responses along the center inline. The shot is at crossline 121 and receiver at crossline 141. Right: Amplitudes of the 3-D migrated impulse responses. The solid lines are theoretical predictions and symbols are the peak amplitudes from the left.

shot and receivers, respectively (see Figure 1), and the hat denotes temporal Fourier transform.

For conventional common-shot migration, we downward continue both shot and receiver wavefields:

$$\begin{cases} \left(\frac{\partial}{\partial z}+\Lambda\right) D = 0, \\ D(x,y,z=0;t) = \delta(\vec{x}-\vec{x_s})\delta(t), \end{cases} \tag{4}$$

and

$$\begin{cases} \left(\frac{\partial}{\partial z}-\Lambda\right) U = 0, \\ U(x,y,z=0;t) = Q(x,y;t) \end{cases} \tag{5}$$

where D and U are the downgoing and upgoing waves (Claerbout, 1985), respectively, and

$$\Lambda = \frac{1}{v}\frac{\partial}{\partial t}\sqrt{1-\left(\frac{\partial^2}{\partial x^2}+\frac{\partial^2}{\partial y^2}\right)\left(\frac{1}{v^2}\frac{\partial^2}{\partial t^2}\right)^{-1}}$$

is the square-root operator. To produce the image, we use the imaging condition

$$R(x,y,z) = \int \frac{\hat{U}(x,y,z;\omega)}{\hat{D}(x,y,z;\omega)}d\omega. \tag{6}$$

For a $v(z)$ medium, Zhang et al. (2001) give an asymptotic expression for the one-way wave fields:

$$\hat{D}(x,y,z;\omega) \sim \frac{i\omega}{2\pi}e^{-i\omega\tau_s}\sqrt{\frac{\cos\alpha_s}{\psi_s\sigma_s}} \tag{7}$$

and

$$\hat{U}(x,y,z;\omega) \sim \iint \frac{i\omega}{2\pi}\sqrt{\frac{\cos\alpha_r}{\psi_r\sigma_r}}e^{i\omega\tau_r}\hat{Q}dx_r dy_r. \tag{8}$$

Substituting (7) and (8) into (6), we obtain

$$R(x,y,z) \sim \iiint \sqrt{\frac{\cos\alpha_r\psi_s\sigma_s}{\cos\alpha_s\psi_r\sigma_r}}e^{i\omega(\tau_r+\tau_s)}\hat{Q}dx_r dy_r d\omega. \tag{9}$$

Comparing (9) with (3), we conclude that the algorithm (4-6) cannot provide the true amplitude image; even the phase term $i\omega$ is missing.

To see why this happens, we observe that for constant velocity, D and U are not components of the full wave fields p, but rather they are related to p by (Zhang, 1993)

$$D = \frac{1}{2}\left(\Lambda - \frac{\partial}{\partial z}\right)p,$$

$$U = \frac{1}{2}\left(\Lambda + \frac{\partial}{\partial z}\right)p,$$

and

$$D + U = \Lambda p.$$

Therefore from (1) and (2) we have

$$\begin{cases} \left(\frac{\partial}{\partial z}+\Lambda\right) D = \frac{1}{2}\delta(t)\delta(\vec{x}-\vec{x}_s), \\ \left(\frac{\partial}{\partial z}-\Lambda\right) U = \frac{1}{2}\delta(t)\delta(\vec{x}-\vec{x}_s), \\ (U+D)|_{z=0} = \Lambda Q(x,y;t), \end{cases} \tag{10}$$

Attaching physical meaning to D and U, we can reformulate (10) as follows:

$$\begin{cases} \left(\frac{\partial}{\partial z}+\Lambda\right) D = 0, \\ \left(\frac{\partial}{\partial z}-\Lambda\right) U = 0, \\ D|_{z=0} = \frac{1}{2}\delta(t)\delta(\vec{x}-\vec{x_s}), \\ U|_{z=0} = \Lambda Q(x,y;t). \end{cases} \tag{11}$$

Noting that the symbol of Λ in the Fourier domain is

$$\lambda = i\frac{\omega}{v}\sqrt{1-v^2\frac{k_x^2+k_y^2}{\omega^2}},$$

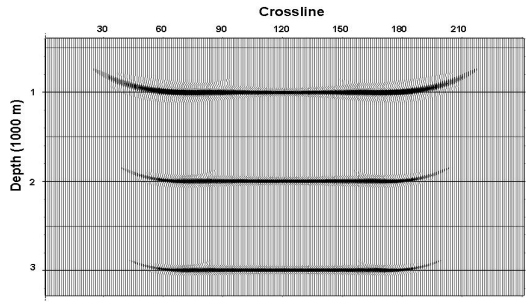

Fig. 3: Flat reflectors along the center inlines after 3-D common shot migration.

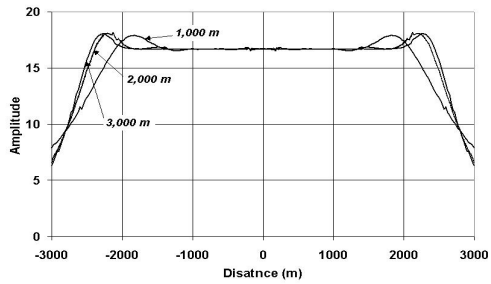

Fig. 4: Peak migrated amplitudes of the three reflectors in Figure 3.

we see that the modified initial condition for U gives an additional phase shift $i\omega$. We also need to modify the imaging condition to be

$$R(x,y,z) = \int \frac{\hat{p}_U(x,y,z;\omega)}{\hat{p}_D(x,y,z;\omega)} d\omega. \qquad (12)$$

Here p_D and p_U are defined as

$$p_D = \Lambda^{-1} D, \qquad p_U = \Lambda^{-1} U,$$

which satisfy $p_D + p_U = p$. It is easy to see p_U and p_D are downgoing and upgoing waves (p^+ and p^-) introduced in Wapenaar (1998). Noticing $\lambda = i\frac{\omega}{v}\cos\alpha$ and applying stationary phase to (11) and (12), we obtain

$$R(x,y,z) \sim \iiint \frac{\cos\alpha_{r0}}{v_0} \sqrt{\frac{\cos\alpha_s \psi_s \sigma_s}{\cos\alpha_r \psi_r \sigma_r}} \; e^{i\omega(\tau_r+\tau_s)} \hat{Q} dx_r dy_r d\omega. \qquad (13)$$

For constant velocity, the splitting (10) is exact. Therefore (11) and imaging condition (12) give the true-amplitude result. This can be directly seen by comparing (13) with (3) and setting $\alpha_{s0} = \alpha_s$, $\alpha_{r0} = \alpha_r$. For the $v(z)$ case, we need to apply another correction term

$$\sqrt{\frac{\cos\alpha_{s0}}{\cos\alpha_s}\frac{\cos\alpha_r}{\cos\alpha_{r0}}},$$

or

$$\sqrt{\frac{\lambda_{s0}}{\lambda_s}\frac{\lambda_r}{\lambda_{r0}}}.$$

Research is currently in progress on modifying the differential operators in (10) to include this factor in the resulting D and U.

Numerical results

Figure 2 (left) shows the 3-D migrated impulse responses along the center inline from a trace with three 7.5 Hz Ricker wavelets at depth 1000m, 2000m and 3000m, respectively. The source is at crossline 121 and receiver at crossline 141 and trace spacing is 50m in both inline and crossline directions. The medium velocity is 2000m/s. Unlike the kinematic behavior, the amplitudes of the impulse responses are asymmetric, with a bias on the receiver side. The peak amplitudes along the impulse responses are in good agreement with the theoretical prediction shown in Figure 2 (right).

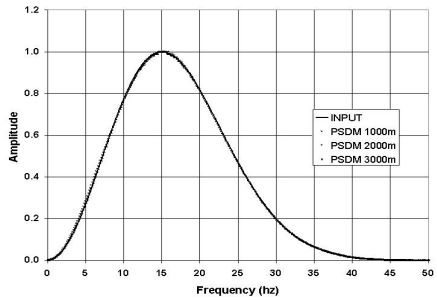

Fig. 5: Frequency spectrum of the migrated wavelets at inline 121 and crossline 121. The solid line is the spectrum of the input 15 Hz Ricker wavelet. The overlay is nearly perfect.

Figure 3 is the center inline of the 3-D migrated result from a single shot over three flat reflectors. The peak amplitudes along the three migrated reflectors are shown in Figure 4. Aside from the edge effects and small jitters caused by interference with wraparound artifacts, the 3-D common shot migration recovers the reflectivity accurately. Figure 5 shows that the frequency content is preserved by the migration at the center trace location. However, the wavelet becomes progressively lower frequency away from the center trace due to the effects of stretching and anti-aliasing.

The next example is from the 3-D SEG-EAGE salt model. The "area shot" dataset was selected over the marine streamer C3-NA dataset because of size considerations. However, this "area shot" dataset is known to produce

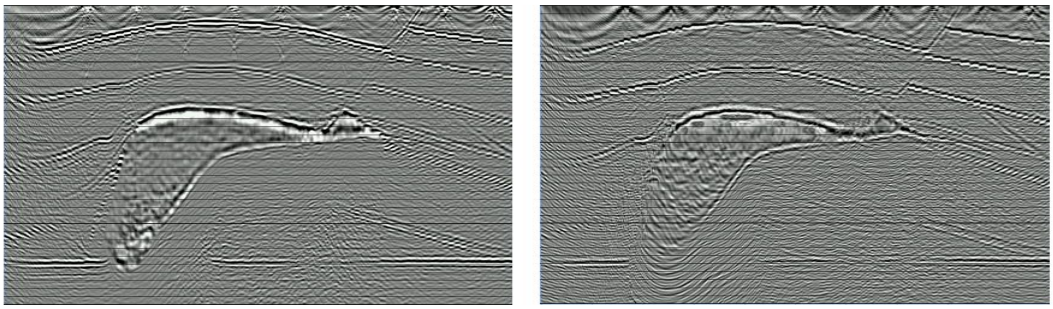

Fig. 6: Inline 242 of the SEG-EAGE model: migrated images from the optimized finite difference algorithm (left) and a single-arrival Kirchhoff migration algorithm (right).

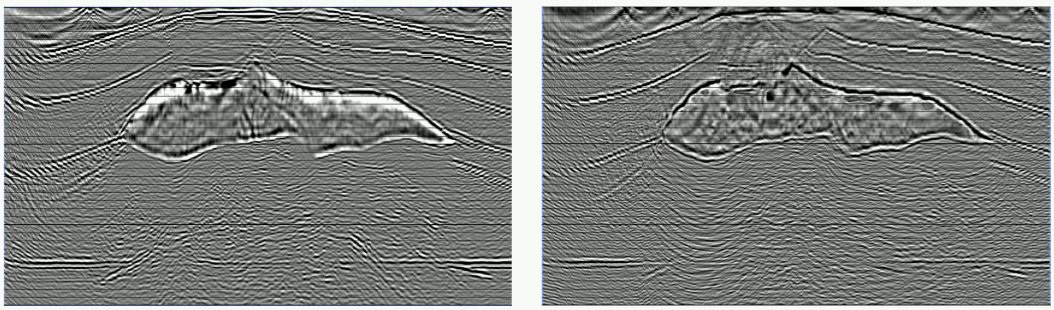

Fig. 7: Inline 342 of the SEG-EAGE model: migrated images from the optimized finite difference algorithm (left) and a single-arrival Kirchhoff migration algorithm (right).

relatively noisy results since it contains only 45 shots. The hybrid finite-difference (Sun et al., 2001) migrated results at inlines 242 and 342, compared with results from the "maximum energy" Kirchhoff migration, are shown in Figures 6 and 7. The finite-difference migrated images show much better imaged salt bottoms. The subsalt flat event images are also significantly improved. Moreover, the finite-difference images do not show the typical "ghost smiles" routinely observed in Kirchhoff-migrated images.

Conclusions

Migrations beased on one-way wavefield extrapolation offer the potential of greater structural imaging quality than single-arrival Kirchhoff migration, but the standard formulation of such migrations, e.g. finite-difference migration, produce incorrect migrated amplitudes. By comparing these amplitudes with those produced by true-amplitude Kirchhoff migration, we have, in effect, calibrated these migration methods, correcting their amplitude and phase behavior.

References

Bleistein, N., Cohen, J. K., and Stockwell, J. W., 2001, Mathematics of multidimensional seismic inversion: Springer.

Claerbout, J., 1985, Imaging the earth's interior: Blackwell Scientific Publications, Inc.

Sun, J., Notfors, C., Gray, S., and Zhang, Y., 2001, 3-D pre-stack common shot depth migration: a structure adaptive implementation: submitted to SEG 2001.

Wapenaar, K., 1998, Reciprocity properties of one-way propagators: Geophysics, **63**, no. 4, 1795–1798.

Zhang, Y., Gray, S., and Young, J., 2000, Exact and approximate weights for Kirchhoff migration: 70th Ann. Mtg., Soc. Expl. Geophys., Expanded Abstracts, **II**, 1036–1039.

Zhang, Y., Gray, S., and Young, J., 2001, True-amplitude common-offset, common-azimuth $v(z)$ migration: submitted to Journal of Seismic Exploration.

Zhang, G. Q., 1993, System of coupled equations for upgoing and down-going waves: Acta Math. Appl. Sinica, **16**, no. 2, 251–263.